Landscape structure and use, climate, and water movement in the Mekong River basin

Mariza C. Costa-Cabral,[1][†] Jeffrey E. Richey,[2][*] Gopi Goteti,[1][‡] Dennis P. Lettenmaier,[1] Christoph Feldkötter[3] and Anond Snidvongs[4]

[1] *Department of Civil and Environmental Engineering, University of Washington, Seattle, WA 98195, USA*
[2] *School of Oceanography, University of Washington, Seattle, WA 98195, USA*
[3] *Mekong River Commission Secretariat, Sikhottabong District, Vientiane 01000, Lao PDR*
[4] *South-east Asia START Global Change Regional Centre, Chulalongkorn University, Bangkok, 10330, Thailand*

Abstract:

In this article the relative roles of precipitation and soil moisture in influencing runoff variability in the Mekong River basin are addressed. The factors controlling runoff generation are analysed in a calibrated macro-scale hydrologic model, and it is demonstrated that, in addition to rainfall, simulated soil moisture plays a decisive role in establishing the timing and amount of generated runoff. Soil moisture is a variable with a long memory for antecedent hydrologic fluxes that is influenced by soil hydrologic parameters, topography, and land cover type. The influence of land cover on soil moisture implies significant hydrologic consequences for large-scale deforestation and expansion of agricultural land. Copyright © 2007 John Wiley & Sons, Ltd.

KEY WORDS   land cover and use change; runoff and stream-flow; south-east Asia; Mekong River basin; macro-scale hydrologic model; soil moisture antecedent conditions

Received 31 August 2005; Accepted 26 February 2007

INTRODUCTION

How a landscape that is evolving in its land cover and use interacts with a variable and changing climate to produce its hydrologic regime is one of the most salient contemporary issues in the face of global change. A particularly sensitive region is south-east Asia, where rapid population growth and socio-economic development over the past several decades has been accompanied by extensive deforestation, expansion of agriculture and irrigation, and stream-flow regulation. In the largest south-east Asian river basin, the Mekong ($795,000$ km^2; Figure 1), with a growing population of 75 million people, forests have been extensively replaced by agricultural land, irrigation has expanded and intensified, and large dams have been constructed for irrigation and hydropower purposes. The Mekong River basin has one of the world's largest freshwater fisheries resources (MRC, 1997), which is vulnerable to altered seasonal stream-flows, sediment load, and changes in water quality. Monsoonal rainfall, which falls in May through October (and represents 80–90% of the annual total), varies markedly from year to year, as does stream-flow. While production of rice, the dominant crop in the region, relies on seasonal flooding, floods are in some years devastating, carrying large human and economic costs. Spatial contrasts in rainfall totals are equally marked, with the eastern and northern highland regions of Laos and the mountains in south-west Cambodia capturing much of the monsoonal rain, and imposing occasionally damaging dry conditions across Thailand's agriculturally-intensive Korat Plateau. Periodically severe droughts in this region cause crop losses, reservoir depletion, low flows, fish kills, and water quality deterioration. Conflicting demands for freshwater resources are increasing throughout the basin. Climate change predictions are that temperature and rainfall in south-east Asia will rise over the twenty-first century in all seasons. According to IPCC (2001), the mean annual temperature rise is expected to be in the order of 1 °C by year 2020, 2 °C by 2050, and 3 °C by 2080; while predicted changes (increases) in mean annual precipitation are about 2% by 2020, 4% by 2050 and 8% by 2080 (as inferred from an ensemble of data generated in experiments with four major climate models). Whetton *et al.* (1994, cited by IPCC, 2001) conclude with high confidence that rainfall will have higher intensity. These important changes have unstudied hydrological consequences.

Determining how landscape structure (topography, vegetation, soils) and climate at regional scales interact to produce discharge regimes in large river basins is thus a scientific challenge, and one with important policy implications. The intent of this work, published in this and a companion paper Costa-Cabral *et al.* (to be submitted) is to evaluate the causes of stream-flow space-time variability in the Mekong River basin, and to use that

---

* Correspondence to: Jeffrey E. Richey, School of Oceanography, University of Washington, Seattle, WA 98195, USA.
E-mail: jrichey@u.washington.edu
† Present address: Hydrology Futures, Seattle WA 98103, USA.
E-mail: cabral@hydrologyfutures.com.
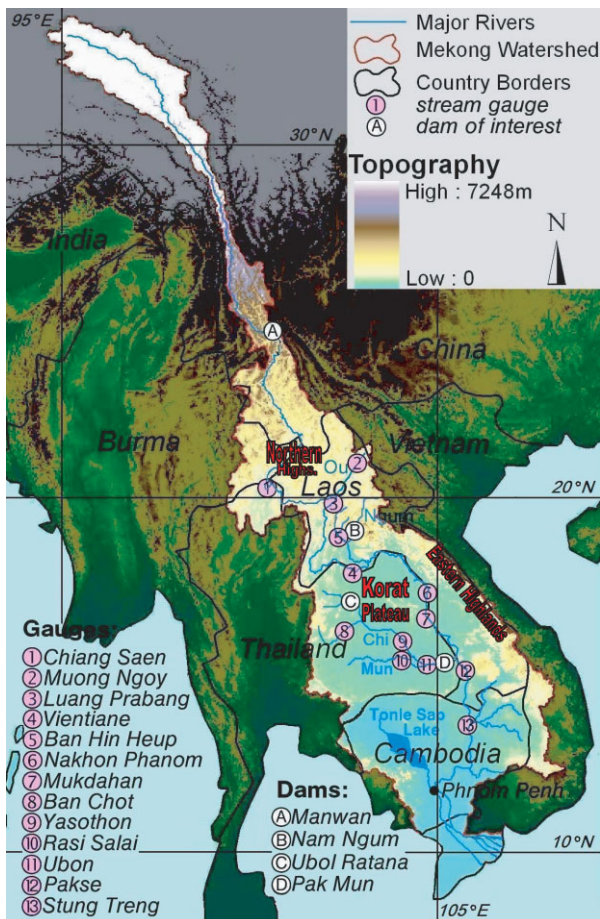‡ Present address: Department of Earth System Science, University of California, Irvine, CA 92697, USA.

Figure 1. The Mekong river basin topography, major streams, location of stream gauges, and location of dams operating in the simulation period (1979–2000)

understanding to predict the basin's hydrologic response to changes in land cover/use and climate. In particular, the relative contributions of space-time variability of rainfall and landscape characteristics (topography, soils, and vegetation) are evaluated in determining regional patterns of soil moisture and the resultant space-time variability in stream-flow. An approach relying solely on observation-based estimates cannot provide sufficient insight into the causes of runoff variability. Interpretation of flow measured at a stream gauge in a particular day is difficult, considering that it includes runoff generated at different dates at nearby and remote locations upstream. Time-aggregated records (monthly or annual), however, provide no information about rainfall intensity, hence its role cannot be explored. Furthermore, empirical approaches are not well suited to evaluation of the role of factors other than precipitation in runoff generation.

Resolution of these questions calls for the application of a spatially distributed hydrologic model which, if appropriately constructed, can capture the effects of space-time variation in precipitation, as well as landscape characteristics, on the genesis of stream-flow. Kite (2001) applied the SLURP hydrologic model to the Mekong basin. Subsequently, Yang and Musiake (2003) applied a model that includes sub-grid parameterizations of runoff generation mechanisms based

on hillslope scale morphology, soil and land cover and use.

The goal of this paper is to simulate and analyse hydrologic responses in the Mekong River basin to those factors which most influence spatial and temporal runoff variability, using the best available geophysical datasets, for a 22-year period (1979–2000). To that end, we use the Variable Infiltration Capacity (VIC) model (Liang *et al.*, 1994; Nijssen *et al.*, 1997, 2001a,b), a macro-scale hydrologic model that is intended specifically for the purposes of representing interactions of land cover, climate, and runoff generation. Slightly different versions of the VIC model than the one we use here have been applied to the Mekong basin by Jayawardena and Mahanama (2002). In the companion paper Costa-Cabral *et al.* (to be submitted), we will use the same model and data sets, to study changes in land cover/use and in climate on runoff generation in the river basin, through the use of scenarios.

METHODOLOGY

In this section, we summarize the biophysical characteristics of the Mekong River basin, and then describe the landscape attributes required by the VIC model, and how they were acquired. These input data sets define the view of the landscape as captured by the VIC model, and are important determinants of the hydrologic predictions of the model.

The VIC model was run at a daily time step for the period 1979–2000. This period was partitioned into a 1979–1988 period used for model parameter estimation (calibration) and the period 1989–2000 used for model evaluation. The greatest changes in land cover and use occurred prior to the 1980s (e.g. MRC, 1997). Deforestation and agricultural expansion continued throughout the 1980s and 1990s (our simulation period), but was then limited to small, less agriculturally suitable areas, the best arable land having been claimed prior to the 1980s (e.g. Fukui *et al.*, 2000).

The Mekong River Basin

The Mekong River basin is the world's eigth largest in discharge (ca. 475 km^3 $year^{-1}$), 12th largest in length (ca. 4800 km), and 21st largest in drainage area (ca. 795 000 km^2). The headwaters of the Mekong River (Figure 1) are in the Tibetan Highlands, at nearly 5000 m elevation. Fed by melting snow, the Mekong runs down the steep Tibetan slopes through a narrow gorge in the Yunnan province of China. The Mekong drainage area is partitioned as follows: 21% in China, 3% in Burma, 25% in Laos, 23% in Thailand, 20% in Cambodia, and 8% in Vietnam. The portion of the basin lying within China, Burma, and the northern part of Laos, consists of mountainous terrain between 400 and 5000 m elevation and is referred to as the Upper Mekong Basin (189 000 km^2), while the remaining 606 000 km^2 of its drainage area form the Lower Mekong Basin.

The 'Northern Highlands' include the region from southern Yunnan province in China through Burma, Laos, and Northern Thailand, and eastward into the northern end of the Annamite Range in Vietnam. The 'Eastern Highlands' mostly consist of the western slope of the Annamite Range shared by Laos and Vietnam. Next to western Cambodia, which receives, on annual average, over 3000 mm of rainfall (according to our estimates later in this paper), the Northern and Eastern Highlands, with elevations of up to about 2800 m, are the wettest regions in the basin. The high mountains have deep-cut valleys and topsoil consisting of a thin deposit of sandstone and igneous rocks. In contrast, the Korat Plateau, comprising the north-eastern region of Thailand, is a dry region. Despite annual rainfall totals between 1000 and 1600 mm, the rainless season lasts from October to April and evapotranspiration is high. The Plateau is mainly drained by the Chi and Mun rivers and includes areas of sandy and some saline soils.

The VIC model

The VIC model is a semi-distributed grid-based macro-scale hydrologic model (Liang *et al.*, 1994; Nijssen *et al.*, 1997, 2001b), which represents explicitly the effects of vegetation, topography, and soils on the exchange of moisture and energy between land and atmosphere. As compared with other so-called soil-vegetation-atmosphere transfer schemes (SVATS), VIC represents in more detail the generation of stream-flow, and its sensitivities to the earlier factors.

The VIC model has been applied to the major river basins of the US (Abdulla *et al.*, 1996; Cherkauer and Lettenmaier, 1999; Maurer *et al.*, 2002; Nijssen *et al.*, 1997); the entire country of China (Su and Xie, 2003); and the pan-Arctic region (Su *et al.*, 2006). Some studies had the purpose of evaluating and improving model parameter estimates. Among such studies are Liang *et al.* (1994), who evaluated the energetics of the model using tower flux data from sites in the central US grasslands, a drained agricultural field in Europe, and a cleared tropical forest site in Brazil. Nijssen *et al.* (1997), evaluated VIC model performance for the Columbia and Delaware Rivers in the US, and demonstrated the ability of the model to reproduce observed stream-flows. Maurer *et al.* (2002), applied the model over the continental US and evaluated its performance using observed stream-flow for many large US river basins. Nijssen *et al.* (2001a), applied the model globally, and showed good reproduction of observed stream-flow in many, though not all, cases. In particular, Nijssen *et al.* (2001a) demonstrated the ability of the VIC model to reproduce the observed seasonal cycle of soil moisture at a number of sites across Eurasia as well as its ability to reproduce seasonal variations in the part of the northern hemisphere covered by snow. The VIC model has been widely used for studies of land surface climate teleconnections (e.g. Zhu *et al.*, 2005), climate change assessments (Payne *et al.*, 2004; van Rheenen

et al., 2004; Christensen *et al.*, 2004), and land cover change studies (Matheussen *et al.*, 2000), among other purposes.

The VIC model can be operated in either one of two modes: in the energy balance mode, the surface energy budget is closed by iterating over an effective surface temperature. Energy balance mode is used, for instance, in coupled land-atmosphere applications, where the model construct requires consistency between the atmospheric and land surface energy, as well as water balances. In water balance mode, which is more typical of hydrologic applications, the effective surface temperature is approximated by the surface air temperature, which avoids the need for iteration and makes the model considerably more computationally efficient. In this study, the model was run in water balance mode. A model grid resolution of $1/12°$ (5 arc-minutes; roughly, 10×10 km^2) of latitude and longitude was used. This choice was dictated by a compromise between the density of the *in situ* (primarily precipitation) data available to drive the model, and the inherent spatial variability of land surface characteristics that the model is intended to represent.

In the VIC model, the subsurface is characterized vertically by three soil layers. The top soil layer contributes to runoff via fast response mechanisms ('quick-flow'), and the deepest soil layer produces base-flow. Drainage between the soil layers is modelled as gravity driven. Controls of vegetation on evapotranspiration are represented explicitly using a Penman–Monteith formulation (Liang *et al.*, 1994). Base-flow is represented as a non-linear recession (Dümenil and Todini, 1992). Sub-grid variations in precipitation rate and temperature, due to variations in elevation, are represented by sub-dividing each grid cell into elevation bands. The effects of snow accumulation and melt are represented using an energy balance snow model described in Cherkauer and Lettenmaier (1999). Daily precipitation, maximum and minimum temperature, and wind speed are the primary meteorological variables that drive the model. Downward solar and longwave radiation, and dew point temperature, also used to force the model, are derived using algorithms that relate them to either the daily temperature, the temperature range, or both (Maurer *et al.*, 2002). Hourly temperatures are estimated by fitting a spline function to the time series of daily minimum and maximum temperatures (Nijssen *et al.*, 2001a). Daily precipitation inputs are distributed uniformly in time throughout the day. The implications of this assumption were tested by Maurer *et al.* (2002) for the Mississippi River basin, and found to be small.

The model used to simulate the routing of stream-flow along the stream network (Lohmann *et al.*, 1996, 1998) uses a triangular unit hydrograph and linearized St Venant's equations to route the stream-flow from each individual grid cell separately to the basin outlet through the channel network. The routing model does not account for channel losses, extractions, or diversions. Simple models were used to represent the operation of reservoirs

and the practice of irrigation and use of bunded fields. These models are described later.

Representation of water use and the surface water balance in paddy fields

Whether irrigated or rainfed, rice paddies are generally surrounded by earth bunds that trap what would otherwise become surface runoff lost to a stream. This retained runoff contributes to increased infiltration, evaporation, and plant transpiration. The VIC code was modified to compute the water balance over the paddy and use it to update the surface storage (ponded water). Haddeland *et al.* (2006) also used a modified VIC code to represent irrigation. In that model, irrigation water is added whenever soil moisture drops below the level where transpiration becomes limited, and continues until moisture reaches field capacity. In our model, irrigation water is added whenever ponded water over an irrigated paddy field is less than 150 mm in depth. According to Apichatvullop (1995), the desirable water depth in paddy land is 150 mm and '[w]hen the depth is less than this, farmers will divert stream water if possible, into the command [irrigated] area.' The change in surface storage from one day to the next is given by the balance between the input (the variable termed incoming flow) and the outputs (infiltration and evapotranspiration). In the original code, the incoming flow equals the precipitation rate (corrected for the fractional area of the grid cell that receives precipitation). In the modified code, an additional quantity may be added to the precipitation rate to make up a larger incoming flow. Whenever there is water ponded over the paddy, the modified code uses the air temperature-dependent value of pan evaporation to compute evaporative losses. In the case of fields classified as non-irrigated (a fraction of agricultural land cover classes 21 and 22), which are mostly rainfed, the incoming flow will be larger than the direct precipitation rate only when surface runoff is generated. When the soil becomes saturated, surface runoff is indeed generated, and because it is retained over the field rather than being allowed to exit into a stream, it is added to the precipitation making up a larger incoming flow. In both irrigated and rainfed paddies, the amount of water in surface storage is limited to a maximum of 150 mm. If surface storage is at its maximum, then any additional incoming flow leaves the bunded field as surface runoff.

Basin topography and river network inputs

Runoff simulated by VIC is routed from each model grid cell to one of its eight neighbouring cells, according to the estimated local flow direction (Lohmann *et al.*, 1996, 1998). The VIC routing network (Figure 2) was defined using methods described in (O'Donnell *et al.*, 1999), from the GTOPO30 data set of the US Geological Service (30 arc second resolution; http://edcdaac.usgs.gov/gtopo30/gtopo30.html), aggregated to the model grid resolution of 5 arc-minutes latitude and longitude. This approach is similar to that used in most of the previous applications of the VIC model cited earlier.

Figure 2. Mekong 1/12° (5 arc-minutes) resolution stream network, used for the routing of simulated runoff

Soil texture and hydrologic parameters

The soil parameters required by the VIC model for each soil layer are the saturated hydraulic conductivity (K_s), porosity (θ_s), field capacity (θ_c), wilting point (θ_w), and parameter n in the Brooks–Corey equation for unsaturated conductivity (Brooks and Corey, 1966). The soil parameters were estimated based on US Department of Agriculture (USDA) soil texture classes, using the conversion values by Schaake (2000). The Brooks–Corey n was obtained from the b parameter in Schaake's table, which represents the slope of the moisture retention curve, in log space, using the relation $n = 3 + 2b$ (see, e.g. Rawls *et al.*, 1993, table V.1·1). Soil texture classes were obtained from soil type as described later.

In this study, the top layer depth was set to 10 cm, and the depths of the second and third layers were established by calibration to observed hydrographs. The available

soil texture data (see later) are partitioned into above and below 10 cm depths, making this a logical choice for the upper layer. Model sensitivity to the upper layer depth was found to be much less than to the depth of the second and third layers. For soil type, we used primarily a map by the Mekong River Commission (MRC, 2003), covering the Lower Mekong Basin, which utilizes the Food and Agriculture Organization (FAO) 1988 classification. This map is in polygon format and was converted to gridded format at 5 arc-minutes resolution in order to match the model grid used. Where re-classification of the MRC data into the FAO-1979 classes (required to use the soilprogram, later) was not feasible, the FAO/UNESCO digital soil map of the world (FAO, 1995), was used. Soil texture (%clay and %sand) and bulk density (ρ_b) were derived from the soil type map using the World Inventory of Soil Emission (WISE) potentials pedon data base (Batjes, 1995) with the aid of the soilprogram (Carter and Scholes, 1999). The methods used to derive soil parameters from this data set are described in (Nijssen *et al*., 1997). From %clay and %sand, each of our 5 arc-minutes pixels was assigned one of the 12 USDA soil texture classes for the top soil layer (<10 cm) and bottom soil layers (>10 cm) (Figure 3).

Land cover

While land use changes in the Mekong River basin clearly occurred during our simulation period 1979–2000, their quantification is difficult. No reliable estimates of deforestation rates are available for the basin. Different data sources, including satellite sources, are generally not mutually compatible, and sometimes disagree due to seemingly subtle differences in processing methods, and to sensor characteristics. The exception is the data set for 1993–1997 by the Forest Cover Monitoring Project (Stibig, 1999) which yielded a rate of net loss of forest of 0·53% per year over the basin for those 4 years. Relative to the entire 1979–2000 simulation period, this rate is probably high, but if we were to apply it, it would imply a net change in forest cover of about 11% from the beginning to the end of our reference period, and of about 5% on average between our calibration and evaluation periods.

For estimation of land cover during our study period, we used the data set prepared by the MRC (2001) for the Lower Mekong Basin (for which 1997 is the base year) combined with GLC2000 products (European Commission, 2003) for the upper basin (for which 2000 is the base year). Figure 4 shows the land cover map used in our simulations. This map was obtained as a composite of the four maps (a)–(d), described later; hence data resolution differs for the Upper Mekong Basin (30 arc-seconds, or roughly 1 km) and the Lower Mekong Basin (0·0012°, or about 250 m). In all cases, the spatial resolution of the land cover is much higher than the spatial resolution at which the VIC model was applied (ca. 10 km), hence the implications of the differences in resolution are modest, given that the VIC model requires only information about the fraction of each of its grid cells covered by a given vegetation type.

The four maps were:

(a) For the Lower Mekong Basin, the 1997 land cover map, with a resolution of 0·0012°, produced by the MRC (2001) in cooperation with the German *Gesellschaft für Technische Zusammenarbeit* (GTZ). The methods used to produce this map were described in Stibig (1999). This map is henceforth designated the 'MRC/GTZ map' and represents the year 1997. The methods used to produce this map combined field observations, aerial photographs, and multi-seasonal satellite images at a 1 : 250 000 scale (Stibig, 1999).
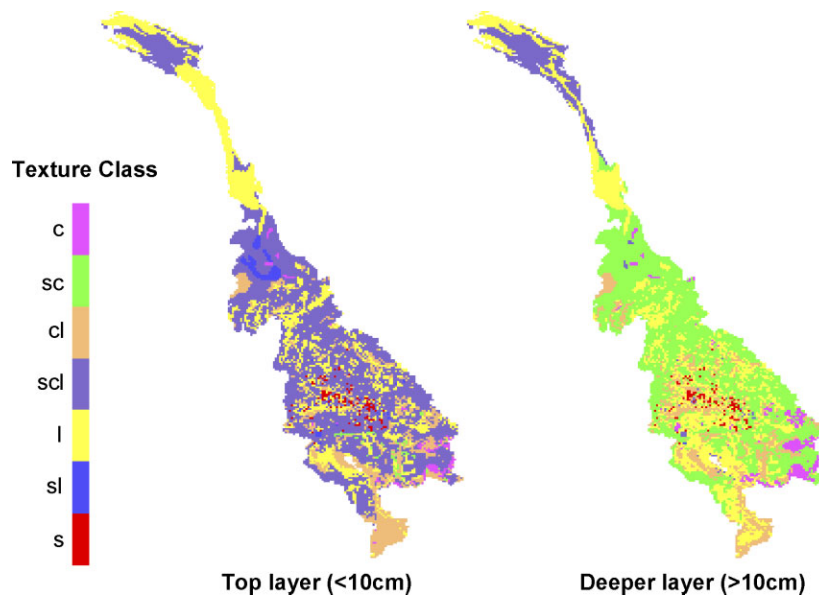

Figure 3. USDA soil texture class. (a) Top layer (<10 cm). (b) Deeper layer (>10 cm). Classes are the following: c, clay; cl, clay loam; scl, sandy clay loam; l, loam; sl, sandy loam; s, sand
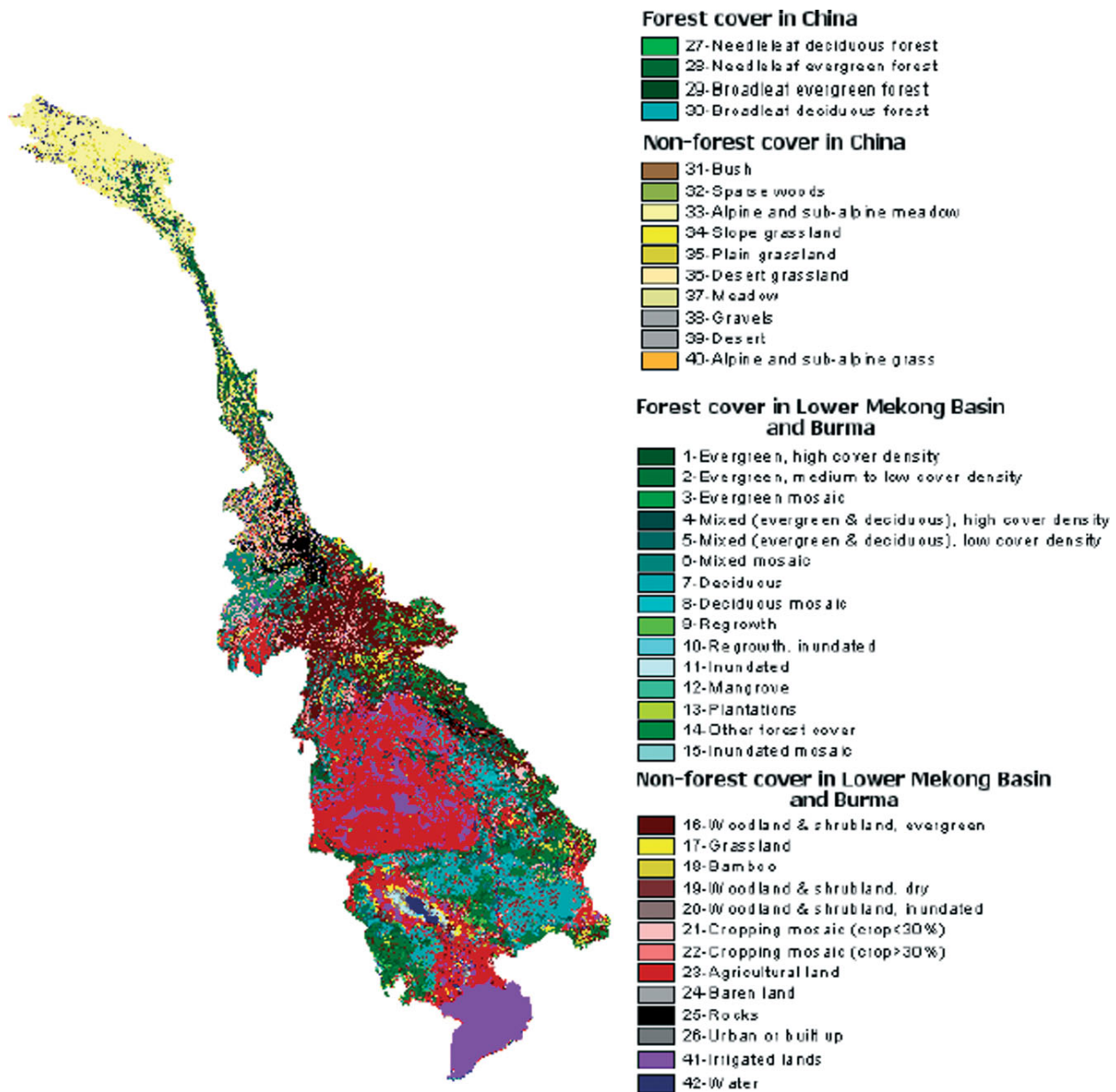
Forest cover in China

- 27- Needleleaf deciduous forest
- 28- Needleleaf evergreen forest
- 29- Broadleaf evergreen forest
- 30- Broadleaf deciduous forest

Non-forest cover in China

- 31- Bush
- 32- Sparse woods
- 33- Alpine and sub-alpine meadow
- 34- Slope grassland
- 35- Plain grassland
- 36- Desert grassland
- 37- Meadow
- 38- Gravels
- 39- Desert
- 40- Alpine and sub-alpine grass

Forest cover in Lower Mekong Basin and Burma

- 1- Evergreen, high cover density
- 2- Evergreen, medium to low cover density
- 3- Evergreen mosaic
- 4- Mixed (evergreen & deciduous), high cover density
- 5- Mixed (evergreen & deciduous), low cover density
- 6- Mixed mosaic
- 7- Deciduous
- 8- Deciduous mosaic
- 9- Regrowth
- 10- Regrowth, inundated
- 11- Inundated
- 12- Mangrove
- 13- Plantations
- 14- Other forest cover
- 15- Inundated mosaic

Non-forest cover in Lower Mekong Basin and Burma

- 16- Woodland & shrubland, evergreen
- 17- Grassland
- 18- Bamboo
- 19- Woodland & shrubland, dry
- 20- Woodland & shrubland, inundated
- 21- Cropping mosaic (crop<30%)
- 22- Cropping mosaic (crop>30%)
- 23- Agricultural land
- 24- Baren land
- 25- Rocks
- 26- Urban or built up
- 41- Irrigated lands
- 42- Water

Figure 4. Composite land cover map of the Mekong basin, combining four different maps (see text). Classes 21, 22 and 23 (cropping mosaics and agricultural land) are also present in the Chinese region

In the legend of Figure 4, classes numbered 1–26, and 43, are taken from the legend of the MRC/GTZ map.

(b) For the irrigated areas in the Lower Mekong Basin, the 'irrigated lands 2001' data of the Atlas by the MRC and WWF (2003). Class 42 in the legend of Figure 4 represents this map.

(c) For the Chinese portion of the Upper Mekong Basin, the 20 arc-second resolution land cover map of the Global Land Cover 2000 (GLC2000) map for China (European Commission, 2003), which was produced from satellite data collected from January to December of 2000, by SPOT Vegetation S10. The GLC2000 maps use the United Nations Food and Agriculture Organization Land Cover Classification System (FAO-LCCS) (http://www.gvm.jrc.it/glc 2000/legend.htm). Classes numbered 27–41 in Figure 4 are taken from this map.

(d) For the Burmese portion, the 30 arc-second resolution land cover map of the GLC2000 map for southeast Asia (European Commission, 2003), which was produced from the satellite SPOT Vegetation S10 data using dry-season images (January to March) for 1999/2000. Similarly to (c), it uses the FAO-LCCS. This map was chosen over the MODIS 2000 satellite-derived map because, judged visually, it is in best agreement with the MRC/GTZ map over the Lower Mekong Basin. Only two land cover classes are represented in the Burmese portion of the Mekong: the class designated 'tree cover, broadleaved, evergreen, closed and closed to open' was assigned to MRC/GTZ class 1, 'Evergreen forest, high cover density'; and the class designated 'cultivated and managed, non-irrigated (mixed)' was assigned to MRC/GTZ class 23, 'agricultural land'.

Vegetation parameters

Leaf area index. The leaf area index (LAI) is a non-dimensional variable that represents the average (projected) leaf surface area covering each unit ground area. LAI is one of the vegetation parameters to which VIC is most sensitive. It controls not only precipitation (solid and liquid) interception, but also canopy resistance to transpiration, and the attenuation of solar radiation through the vegetation cover. The standard 8-day, 1 km MODIS satellite LAI product was used (http://modis.gsfc.nasa.gov), monthly averages having been taken over the period 1 March 2000 through 28 February 2001. The 12 monthly mean LAI values thus generated for each model grid cell are shown in Figure 5. The spatial patterns of LAI in Figure 5 show good correspondence with the land cover map in Figure 4, with forest having the highest LAI values, and agricultural land having the lowest. The regions with highest LAI are Laos and Vietnam (with the exception of the Mekong Delta), and some regions of Cambodia far from the Tonle Sap Lake. The Thai portion of the basin has a LAI mostly below 2·0 throughout the year, due to the strong dominance of agriculture there. The high-elevation areas of China's Yunnan province also have a LAI mostly under 2·0 year-round, which is indicative of the sparse vegetation in the upper basin. It was determined that there was a major problem with the MODIS values during the May through October rainy season, probably due to difficulties in obtaining valid satellite readings in the cloudy conditions of this season. Therefore, we decided to use the MODIS LAI values for November 2001 to represent the months from June through October, and the MODIS LAI values for April 2000 to represent the month of May.

Albedo. Albedo has large impact on the VIC computed evaporation from the canopy, and plant transpiration. We based our assignment of seasonal albedo on previous relevant observations elsewhere, mainly from Giambelluca *et al.* (1999), and attempted to correctly represent the albedo values of the vegetation classes relative to each other. In tropical regions, albedo is generally observed to be highest during the dry season because of reduced LAI (Pinker *et al.*, 1980; Barradas and Adém, 1982; cited by Giambelluca *et al.*, 1999), with seasonal variations due to changes in sun angle being relatively unimportant. Annual minimum and maximum albedo values were established for each of the land cover classes in Figure 4, corresponding to the dry season (November–May) and the wet season (June–October), respectively (see Table I). The values used ranged from a low of 0·085 for irrigated cropland (class 41) to 0·6–0·8 for old snow and 0·8–0·9 for new snow (e.g. Gray and Prowse, 1993).

Vegetation height, displacement height, roughness length, and architectural resistance. Vegetation height is used by VIC as the basis for determining roughness length and displacement height, both of which are important parameters in its evapotranspiration formulation. We were unable to identify studies reporting vegetation height for different land cover classes in Mekong regions, except for the approximate values mentioned in Stibig (1999) for classes 7, 9, 10, 16, 19 and 20. Values from Sellers *et al.* (1986) were therefore used for classes 1, 2, 27 and 28. For all other classes, values judged reasonable (from field observations by some of the authors) were utilized (Table I), but which have not been validated. Roughness length is defined as the height above the ground where wind speed is reduced to zero due to surface resistance. This parameter is used to determine the wind profile in VIC using a logarithmic approximation. Displacement height is defined as the height above the ground where wind speed is not significantly affected by surface roughness. Roughness length and displacement height were estimated by multiplying the vegetation height in Table I by the factors 0·123 and 0·67, respectively [following Brutsaert (1975) cited in Shuttleworth (1993, p. 4·12)]. The values used for architectural resistance (R_{arc}, Table I) are based on Ducoudré *et al.* (1993).

Minimum stomatal resistance, RGL, and solar radiation attenuation. The minimum stomatal resistance (R_{min}) is defined as the stomatal resistance that occurs with full sunlight and at saturation leaf water potential. VIC uses R_{min}, together with LAI and current soil moisture, to calculate the canopy resistance to transpiration—based on the formulations of Blondin (1991) and Ducoudré *et al.* (1993), as described in Liang *et al.* (1994). The values of R_{min} used in our simulations are listed in Table I. RGL is the minimum incoming shortwave radiation at which there will be transpiration. For forest cover classes we used the value 30 W m^{-2}, and for agriculture we used 100 W m^{-2}. Intermediate values were used for other land cover classes, as specified in Table I. Solar radiation attenuation was approximated at 50%.
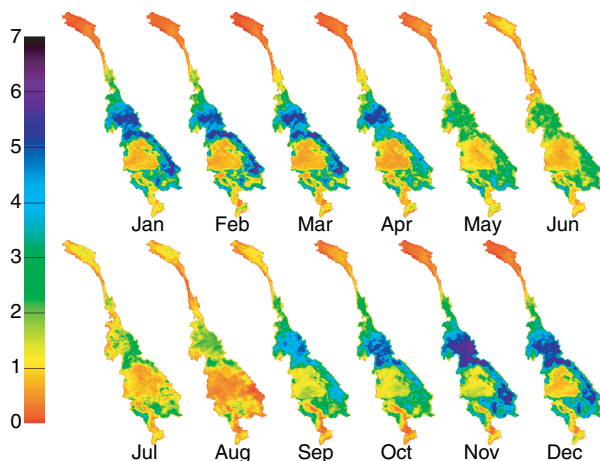

Figure 5. Maps of mean monthly LAI for the Mekong River basin obtained by spatial and temporal aggregation of MODIS data, from March 2000 to February 2001

Table I. Vegetation parameter values adopted in the simulation runs for each land cover class in Figure 4

Land cover class	Albedo		Vegetation height (m)	R_{arc} (s m^{-1})	R_{min} (s m^{-1})	RGL (W m^{-2})	Maximum rooting depth (m)
	Wet season	Dry season					
Forest cover in Lower Mekong Basin and Burma							
1 Evergreen forest, high cover density	0·120	0·120	35	25	80	30	3·0
2 Evergreen forest, medium to low cover density	0·125	0·125	30	25	80	30	3·0
3 Evergreen forest mosaic	0·125	0·125	25	25	80	30	3·0
4 Mixed (evergreen & deciduous), high cover density	0·120	0·125	35	40	100	30	2·5
5 Mixed (evergreen & deciduous), low cover density	0·125	0·130	30	35	95	30	2·5
6 Mixed forest mosaic	0·130	0·140	25	30	90	30	2·5
7 Deciduous forest	0·125	0·135	20	40	80	30	2·0
8 Deciduous forest mosaic	0·135	0·140	15	40	80	30	2·0
9 Regrowth forest	0·150	0·153	8	30	90	30	1·0
10 Regrowth forest, inundated	0·120	0·120	8	20	90	30	1·0
11 Inundated forest	0·120	0·120	15	20	80	30	1·0
12 Mangrove forest	0·120	0·120	10	30	90	30	1·0
13 Plantation forest	0·130	0·135	20	2	80	30	1·0
14 Other forest cover	0·125	0·130	20	30	90	30	2·0
15 Inundated forest mosaic	0·120	0·120	15	2	80	30	1·0
Non-forest cover in Lower Mekong Basin and Burma							
16 Woodland & shrubland, evergreen	0·150	0·155	5	25	110	50	1·0
17 Grassland	0·168	0·171	1	2	80	100	0·5
18 Bamboo	0·147	0·150	10	5	80	100	0·5
19 Woodland & shrubland, dry	0·157	0·160	5	3	110	75	5·0
20 Woodland & shrubland, inundated	0·120	0·120	5	3	90	75	0·5
21 Cropping mosaic (crop <30%)	0·157	0·160[a]	5	2	80	100	0·5
22 Cropping mosaic (crop >30%)	0·162	0·165[a]	5	2	80	100	0·5
23 Agricultural land	0·170	0·170[a]	1	2	80	100	0·5
24 Baren land							
25 Rocks			VICs treatment of 'baren land' was used.				
26 Urban or built up							
Forest cover in Chinese part of Upper Mekong Basin							
27 Needleleaf deciduous forest	0·125	0·350	17	40	80	30	3·0
28 Needleleaf evergreen forest	0·125	0·300	20	50	80	30	3·0
29 Broadleaf evergreen forest	0·125	0·300	35	50	80	30	3·0
30 Broadleaf deciduous forest	0·125	0·350	20	40	80	30	3·0
Non-forest cover in Chinese part of Upper Mekong Basin							
31 Bush	0·155	0·350	2	3	100	75	5·0
32 Sparse woods	0·150	0·350	2	10	100	50	2·5
33 Alpine and sub-alpine meadow	0·200	0·500	0·5	2	80	100	0·5
34 Slope grassland	0·200	0·400	0·5	2	80	100	0·5
35 Plain grassland	0·200	0·400	0·5	2	80	100	0·5
36 Desert grassland	0·200	0·400	0·5	2	80	100	0·5
37 Meadow	0·200	0·400	0·5	2	80	100	0·5
38 Gravel							
39 Desert			VICs treatment of 'baren land' was used.				
40 Alpine and sub-alpine grassland	0·200	0·500	0·5	2	80	100	0·5
Water							
41 Irrigated cropland	0·085	0·085	0·5	2	60	100	0·5
42 Water body			VICs treatment of 'baren land' was used.				

Note: Wet Season and Dry Season are here defined as May-October and November-April, respectively.
[a] In grid cells receiving snow in winter, the winter albedo was set to 0·4 for cropping mosaic classes (21 and 22) and to 0·5 for the agricultural land class (23).

Wind and wind attenuation. The VIC parameter wind height is the height above ground at which wind observations were recorded. VIC expects this measurement to have been made at high enough elevation that the vegetation effects on wind speed are negligible. The model then estimates wind speed through and below the canopy using logarithmic wind profiles. As in Maurer *et al.* (2002) and Nijssen *et al.* (2001b), we used wind speed data from the NCEP-NCAR Reanalysis (Kalnay *et al.*, 1996) and assumed the wind measurement height to be equal to 2 m above the vegetation height in the case of short vegetation classes (of grassland, shrubland, and agricultural land), and equal to 10 m above the vegetation height in the case of tall vegetation classes (forest

classes). Wind speed attenuation through the overstory to a 2 m height was approximated at 50% when a tree canopy is present and at 10% when it is not.

Maximum rooting depth, and distribution of root mass with depth. Maximum rooting depth affects the ability of the vegetation to extract moisture from the three soil layers, and hence affects evapotranspiration. The values of maximum rooting depth used in our simulations are listed in Table I. The bulk of root mass was allocated to the top two soil layers.

Meteorological data

The meteorological data used to drive VIC are daily precipitation, maximum and minimum temperature, and mean wind speed. Other forcing data (e.g. downward solar and longwave radiation, humidity) are derived from the daily temperature or temperature range, as described in Maurer and Lettenmaier (2003). Station observations of daily precipitation and temperature were obtained from the NOAA Climate Prediction Centre Summary of the Day data archived at the National Centre for Atmospheric Research (NCAR) for the period January 1979 through December 2000. Data from 279 stations were interpolated to the 5 arc-minutes model grid cells using the SYMAP algorithm (Shepard, 1984) to obtain daily time series of precipitation and maximum and minimum temperature for each grid cell. Temperature data were interpolated using a lapse rate of $-6.5\,°C\ km^{-1}$ to adjust temperature from the station to each elevation of the grid cell. Wind speed data was interpolated from the NCEP-NCAR Reanalysis data set (Kalnay *et al.*, 1996) to the 5 arc-minutes model grid cells.

Model calibration and verification

Some of the soil parameters in VIC generally cannot be estimated directly, and must be adjusted by calibration. These calibration parameters are: the depth of each soil layer (L_1, L_2, L_3; as said earlier, L_1 was set to 10 cm and only L_2 and L_3 were calibrated); the maximum velocity of base-flow (D_{smax}), which can first be estimated by multiplying the saturated hydraulic conductivity (K_s) by the local terrain slope; the fraction of D_{smax} where non-linear base-flow begins (D_s); and the parameter of the variable infiltration curve (b_{inf}). The sensitivity of model results to each of these parameters is briefly discussed in Nijssen *et al.* (2001b).

Calibration was performed for each sub-basin separately, using the mean monthly flow recorded at each stream gauge (for location of the stream gauges, see Figure 1), following methods outlined in Maurer and Lettenmaier (2003) and Nijssen *et al.* (1997, 2001b). For every gauge located downstream of another, an additional portion of the basin is drained. This additional area was calibrated separately, using the difference in flow rates recorded by the two stream gauges.

Figures 6 and 7 show simulated monthly average flows and observations for each gauge used for calibration. Given the sparseness of rain gauges available, the agreement between the calibrated simulation results, referred to as the 'historical simulation' and the observation-based estimates is reasonable, with a Nash–Sutcliffe index (Nash and Sutcliffe, 1970) of 0·72 for the basin above Stung Treng. Significant disagreements in predicted and observed year-to-year variability can be seen in the smaller sub-basins, especially Ban Chot, where
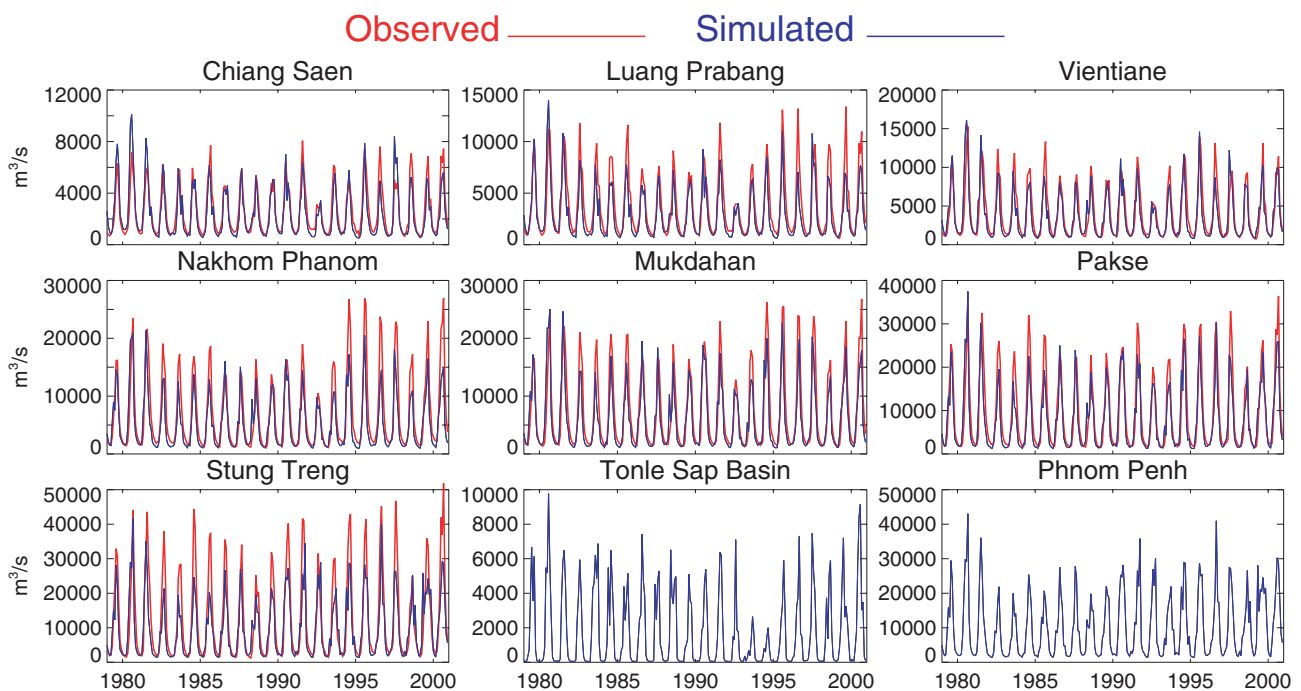

Figure 6. Observed and simulated hydrographs for recording gauges in the mainstem of the Mekong River and the ungauged Tonle Sap river basin, in 1979–2000. The observed hydrographs were calculated by the MRC (personal communication, 2003) using rating curves

agreement could not be improved by any further adjust-ment of the calibration parameters. Small scale rainfall variability is reflected most in such small basins, and is not captured by the rain gauge network. Consequently, the overall reproduction of the records at the 13 stream gauges over the 22 years of simulation (1979–2000) was judged adequate.

Simulated hydrographs were created for two locations where observations were not available: Phnom Penh (just above the confluence with the Tonle Sap River), and the Tonle Sap Lake. In these areas for which calibration was not possible due to lack of observations, soil parameters calibrated for neighbouring areas were used.

ANALYSIS OF HYDROLOGIC FLOW PATTERNS

In this section, the spatial and seasonal patterns of precipitation, simulated runoff and soil moisture are analysed for the simulation period, 1979–2000, and the influence of soil moisture conditions on runoff generation in the VIC model is investigated. Upon establishing this relationship, the effects of land cover on soil moisture are explored.

Spatial and seasonal patterns of precipitation, soil moisture and runoff

Estimated mean monthly and annual precipitation, simulated mean monthly locally generated runoff (without routing) and soil moisture are shown in Figures 8–11. Figures 8 and 9 reveal a distinct rainy season due to the passage of the south-west and the north-east monsoons during May through October, with the highest rainfall occurring in south-western Cambodia (surpassing 3000 mm year^{-1}) and the Eastern Highlands of Laos (2500–3000 mm year^{-1}). Precipitation over the northern part of the Eastern Highlands is also considerable in June-July-August, while in the remainder of the Eastern Highlands the annual peak is in October (Figure 8). The lowest volumes year-round are found in the Himalayan Highlands (roughly 500 mm year^{-1}), falling largely as
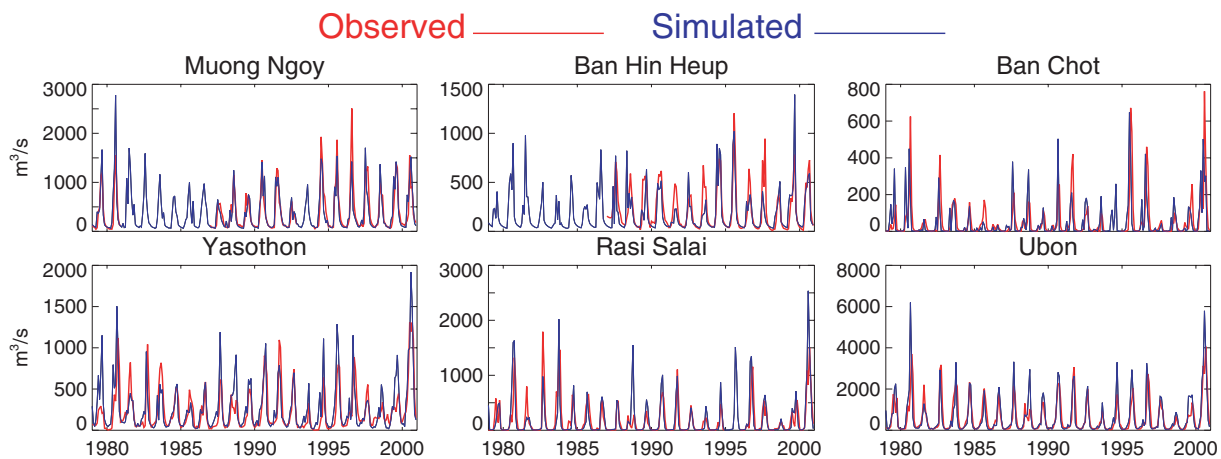
Figure 7. Observed and simulated hydrographs for recording gauges in tributaries of the Mekong River, in 1979–2000. The observed hydrographs were calculated by the MRC (personal communication, 2003) using rating curves
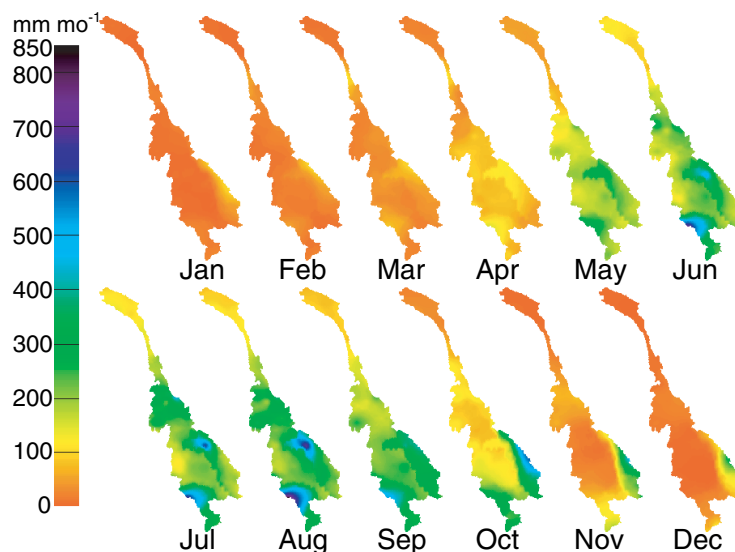

Figure 8. Average monthly precipitation over the Mekong River basin in 1979–2000, obtained by interpolation from the rain gauge network

snow. The Mun-Chi basin in the Korat Plateau in Thailand (100–200 m elevation) is notably dry in terms of runoff (Figure 10), receiving on average an estimated ca. 1300 mm year^{-1} of rainfall but having an extensive rainless season (October through April) and high evapotranspiration. The mountain ranges to the south and west of the plateau capture much of the moisture arriving with the south-west monsoon, while the Annamite Range in Vietnam depletes the north-east monsoon moisture.
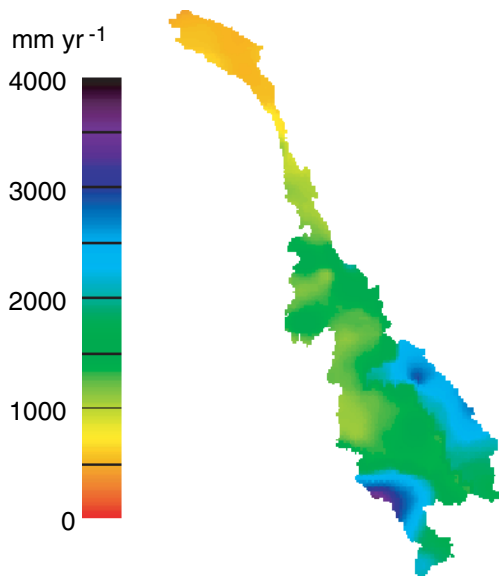

Figure 9. Average annual precipitation over the Mekong River basin in 1979–2000, obtained by interpolation from the rain gauge network

The spatial distribution of soil moisture in the upper two layers, L_1 and L_2, shows the influence of precipitation patterns, as well as topography, and soil texture (Figure 11). The moisture in the deepest soil layer, L_3, however, is more strongly influenced by base-flow and evapotranspiration, which in turn is affected by soil depth,

soil hydrologic parameters, vegetation parameters, and terrain slope. The peak soil moisture in the upper two layers closely follows the seasonal maximum of precipitation (August). The peak is somewhat delayed for L_3 (Figure 11), where soil moisture saturation remains high through November, long after the decline in precipitation. The minimum soil moisture levels are lagged relatively to the minimum precipitation, which occurs in January: it is February–March for L_1 and L_2, and April for L_3.

Such phase shifts at greater soil depths were particularly well documented in a 16-year observed time series of soil moisture from Illinois, US (Wu *et al.*, 2002). Soil hydrology has long been recognized as a low-pass filter for atmospheric forcing (Delworth and Manabe, 1988, 1989). Persistence of soil moisture, in addition to prolonging the effects of floods and droughts (e.g. Bonan and Stillwell-Soller, 1998), also causes persistence in near-surface atmospheric humidity, temperature, and precipitation (e.g. Delworth and Manabe, 1988, 1989; Koster and Suarez, 1995; Eltahir, 1998).

While the Korat Plateau appears as distinctly lower in terms of precipitation (Figures 8 and 9) and runoff (Figure 10) than the surrounding areas in Laos, Vietnam and Cambodia, the same is not true for soil moisture (Figure 11). Soil moisture in the Korat Plateau remains high throughout the rain season as a result of the simulated practice of bunded fields over this agricultural over most of which bunded fields are used (Fukui *et al.*, 2000). Most of these bunded fields are rainfed, and a smaller part—11·5% of the region's area, according to the dataset shown in Figure 4—are irrigated. The practice of irrigation in the Korat Plateau from mid-June through October, mostly adjacent to large streams (Figure 4) is also reflected in the simulated soil moisture. The deepest soil layer, L_3, remains close to saturation throughout the irrigation season. This simulated effect is most marked in the Chi basin above the Yasothon streamgauge, where the calibrated depth of layer L_2,
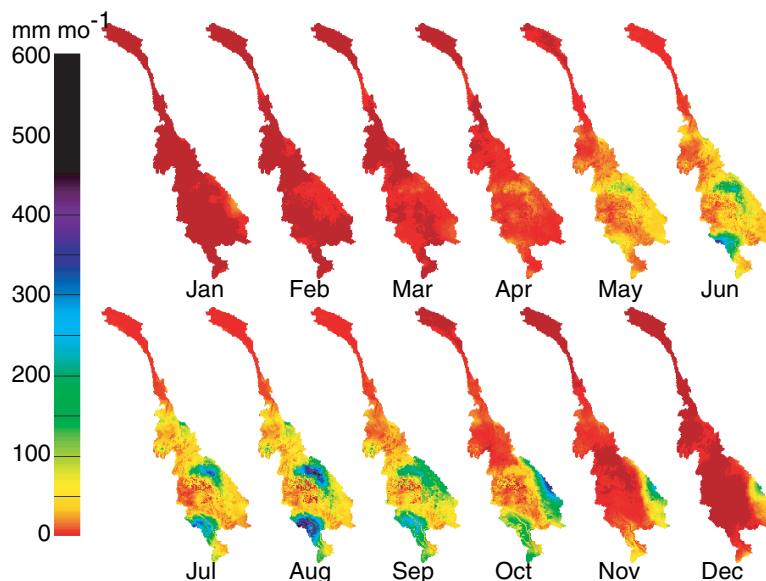

Figure 10. Simulated average monthly runoff in 1979–2000

L1

Jan Feb Mar Apr May Jun

Jul Aug Sep Oct Nov Dec

L2

Jan Feb Mar Apr May Jun

Jul Aug Sep Oct Nov Dec

L3

Jan Feb Mar Apr May Jun

Jul Aug Sep Oct Nov Dec
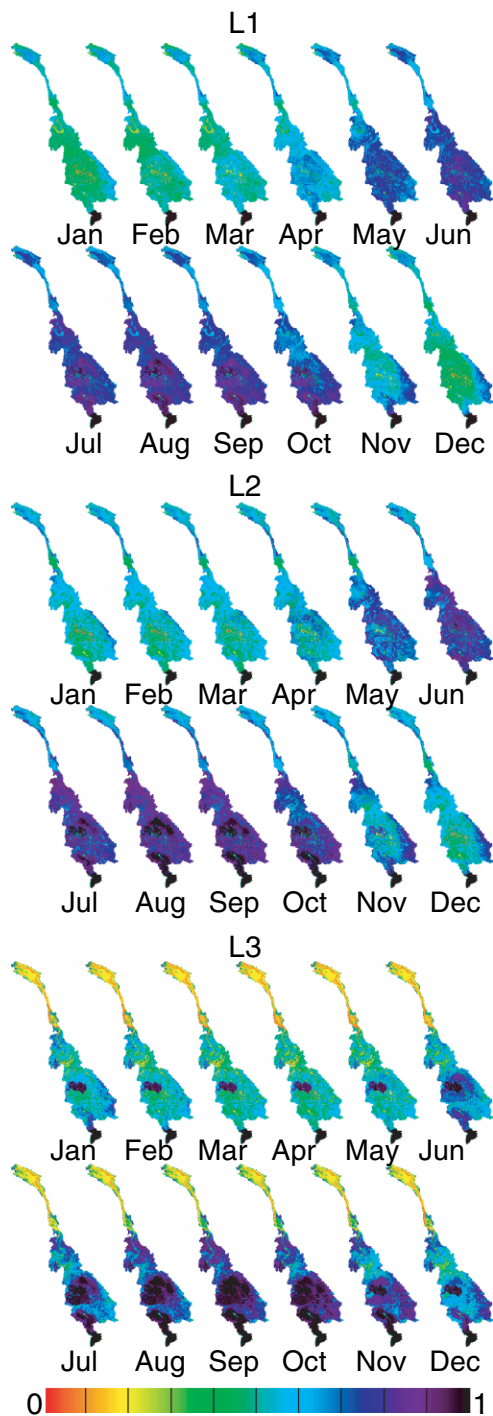
0 |████████████████| 1

Figure 11. Simulated average monthly soil moisture saturation (expressed as a fraction of the maximum water content, established by porosity and soil depth) in 1979–2000, for the surface (L_1), middle (L_2) and bottom (L_3) soil layers

50 cm, is greater than elsewhere in the Korat Plateau (10 cm). Soil layer L_2 in the VIC model acts as a reservoir which replenishes losses by evapotranspiration in the top soil layer, L_1, and losses by base-flow in the deepest soil layer, L_3. Indeed, in the sub-basin above Yasothon L_3 remains at high saturation levels year-round, not just during the irrigation season.

The effects of soil texture on soil moisture are also visible, with several recognizable patterns from Figure 3

appearing in Figure 11. Coarser soil types (sand, dandy loams) drain faster and generally result in lower soil moisture content in L_1 and L_2. The effects of topography are also visible in all three layers, and especially in L_2 and L_3. The monthly soil moisture maps for L_3 have a clear imprint of the major valleys, such as the Mekong River mainstem, and the ridges, such as that which separates the Korat Plateau from Cambodia; and the low-lying low-relief areas surrounding the Tonle Sap Lake have high degrees of saturation during the rain season.

The spatial patterns of simulated runoff generation (before any stream routing; Figure 10) roughly follow those of precipitation (Figure 7), and both have maxima in August. The runoff minimum, however, persists through February and March over most of the basin, beyond the precipitation minimum in January. This is caused by two factors: low antecedent soil moisture, and the interception by the vegetation canopy of rain falling at a low rate. Because bunded fields retain surface runoff in ponded conditions, allowing re-infiltration and increased evapotranspiration, Korat Plateau runoff is notably low even during the rainy season; having an average annual runoff ratio, defined as the ratio of runoff to precipitation, of 0·15, which is considerably lower than the 0·43 average for Mekong River basin as a whole.

Influence of rainfall and soil moisture on runoff generation

Monthly rainfall, at any latitude, has been shown to have little or no memory and to vary at all time scales, with a variability spectrum that is close to white (Hasselmann, 1976). Soil moisture, in contrast, is strongly autocorrelated. The dominant feature of soil moisture spectra is their resemblance to red noise (Delworth and Manabe, 1988, 1989; Vinnikov *et al*., 1996; Entin *et al*., 2000), with characteristic time scales ranging from a few months to a few years. This is a consequence of soil moisture being a storage, representing the balance between accumulated infiltration, evapotranspiration, and base-flow (the latter for the lowest VIC layer only).

In Figure 12, the weekly mean total soil moisture (obtained by adding the moisture of all three soil layers) during the simulated period, 1979–2000, is plotted against that week's precipitation for the following areas: (a) the high elevation sub-basin above Chiang Saen, which has thin soils (calibrated soil depths are no larger than 1 m) and steep slopes; (b) the Mun-Chi River sub-basin in Thailand's Korat Plateau, above Ubon, where slopes are slight; (c) the territory of Laos lying within the Mekong basin, a largely mountainous area with calibrated soil depths of about 1 m; and (d) the entire catchment area above Stung Treng, which encompasses the areas in (a), (b) and (c).

Colour is used in Figure 12 to represent the magnitude of simulated quick-flow (QF; top panels), base-flow (BF; middle panels), and total flow (TF; bottom panels). Arrows are drawn on each panel indicating the direction of fastest increase in flow rate (QF, BF, or TF). The slope of the arrows were computed by bi-linear regression
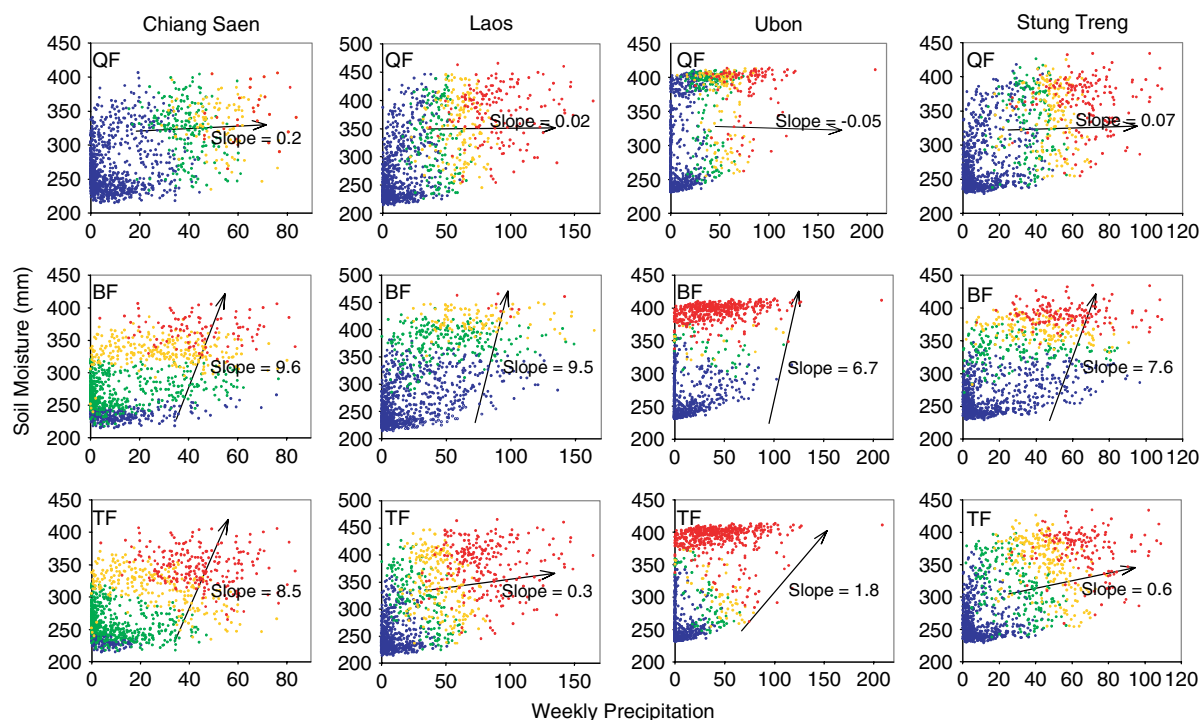
Figure 12. Dependence of quick-flow (QF, top row panels), base-flow (BF, mid-row panels), and total flow (TF, bottom row panels) on weekly mean precipitation total (*x* axis) and soil moisture (*y* axis), for the sub-basin upstream of Chiang Saen, the Mun-Chi basin in Thailand (which drains through Ubon), the Laos territory within the basin, and the sub-basin upstream of Stung Treng (which encompasses Chiang Saen, Laos, and Ubon). In each column, all three panels show the same plotted points, the difference being solely in colour. The colour scale corresponds to the magnitude of simulated flow rate (QF, BF or TF), as indicated in the figure legends. Arrows indicate the mean direction of fastest increase in flow rate, and the slope of each arrow was determined by bi-linear regression of the dependent variable (flow rate) over the two independent variables, precipitation and soil moisture

of the dependent variable, flow rate, over the two independent variables, precipitation and soil moisture. For quick-flow, the arrows are closer to the horizontal than to the vertical at all sites, reflecting a dominant dependence of quick-flow on recent precipitation. The opposite is true for base-flow, with boundaries between colours being almost horizontal at all sites and arrows pointing strongly upward, reflecting the dominance of soil moisture. For total flow, i.e. the sum of quick-flow and base-flow, the arrows are diagonal with moderate slopes, reflecting the dependence of runoff on both precipitation and soil moisture.

The importance of soil moisture to runoff generation is apparent even when the hydrologic response is aggregated to monthly values for this large basin. Figure 13 shows the monthly means of precipitation, simulated runoff, and simulated soil moisture aggregated over the large basin area upstream of Stung Treng (ca. $662\,000$ km^2). The monthly means (the central black line) illustrate that the peak in average monthly soil moisture occurs in September rather than during the peak precipitation month of August. Soil moisture remains high in October and November, despite the steep fall in average monthly precipitation during these months. The soil moisture minimum is particularly lagged, occurring in March–May, with respect to the month of lowest precipitation (January).

In 1980, there were two peaks in monthly precipitation (Figure 13a), the most extreme of which was in June

(309 mm). But it was the smaller peak which occurred in September (279 mm) that generated the highest simulated monthly runoff (Figure 13b). Why was monthly runoff in June 1980 lower than September 1980, and why was the September 1980 runoff so extreme? The answer lies in the soil moisture levels (Figure 13c): rainfall throughout the summer months caused the soils to become more highly saturated in September (547 mm) than it had been in June (439 mm).

The monthly values for 1987, a drought year, are also shown in Figure 13. After four months of below-average precipitation (April–July), above-average precipitation occurred in August and September. Yet the runoff response in those two months was modest compared to 1980. In September 1987, runoff was only about average despite the high precipitation (254 mm, a value not far below that of September 1980). This is likely a consequence of below-average soil moisture in September of 1987 (389 mm), resulting from the low precipitation in April–July.

The year with the highest estimated precipitation in the month of September was 1996 (301 mm). Yet, the total simulated runoff in September of 1996 was only 157 mm, a value below the 163 mm runoff simulated for September of 1980. The soil moisture level over the basin in September of 1996 was only about average (491 mm), while in September 1980 it had reached 547 mm.
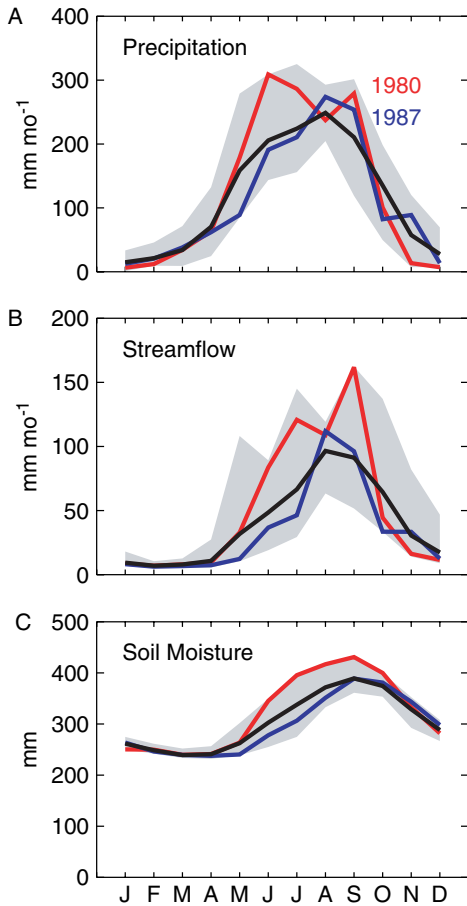
Figure 13. Precipitation, total runoff generated (without stream routing), and total soil moisture above Stung Treng in 1980 and 1987. For each month, the range from minimum to maximum simulated monthly values in 1979–2000 is represented by the shaded area, and the monthly average is plotted in black. Reasons for the different runoff responses to the two monthly precipitation peaks of June and September of 1980, and reasons for the different runoff responses to the two September peaks of 1980 and 1987, are explored in the text
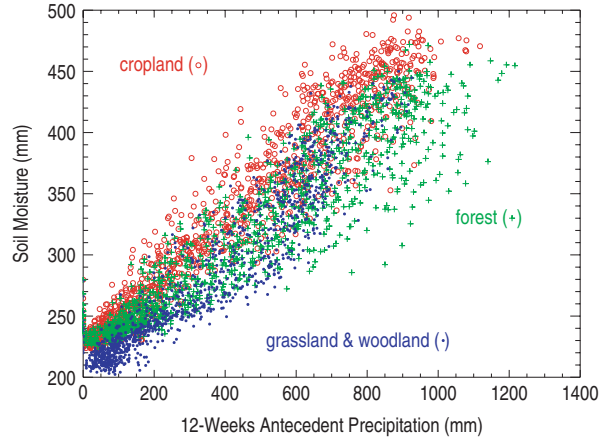

Figure 14. Dependency of average soil moisture in Laos on the total precipitation falling in the 12 preceding weeks, for forest classes, grassland and woodland classes, and agricultural classes. Each plotted point corresponds to 1 week in the simulation period. Irrigated areas were excluded from this plot

Influence of landcover type on soil moisture and runoff generation

Given the influence of soil moisture on runoff generation and the difference in vegetation parameters among the land cover classes, land cover is expected to affect both soil moisture and runoff generation. We examine the territory of Laos, which has a variety of land cover classes. Given that calibrated soil depths are fairly uniform over the territory of Laos (about 1 m), model differences will be due primarily to prescribed differences in vegetation. Figure 14 shows the mean weekly soil moisture as a function of the total precipitation in the preceding 12-week period, for each week of the simulation period, for the three major groups of land-cover classes: (a) forest (to which forest regrowth is aggregated), (b) cropland, and (c) woodland and shrubland (to which the less common grassland is aggregated as well). The classification of 'woodland and shrubland' was assigned in the original dataset to areas with less than 20% tree crown cover (30% in the case of evergreen and mixed forests) or with trees of height under 5 m (Stibig, 1999).

Figure 14 shows that for any given value of antecedent precipitation, soil moisture is generally highest in the portion of Laos where agriculture predominates. This result is explained by the higher rainfall interception and evapotranspiration rates for forests, aided by higher LAI, lower albedo, higher aero-dynamic roughness, and deeper roots. When antecedent precipitation is relatively low, the lowest soil moisture generally occurs where grassland or woodland predominates; and when antecedent precipitation is higher, the lowest soil moisture occurs where forest predominates—which reflects the ability of deeper (relative to other vegetation types) tree roots to extract deep soil moisture.

Interpretation of Figure 14 is however not straightforward because, within Laos, land cover classes, like rainfall and temperature, are correlated with terrain elevation, slope, and slope orientation. However, VIC does not represent slope effects directly—they are only represented indirectly through the *b* parameter (which controls partitioning of precipitation into quick-flow and infiltration into the upper layer, but which also reflects various other heterogeneities besides topography) and, in our simulations, also through the D_{Smax} parameter (which controls the maximum velocity of base-flow). Hence, differences in VIC simulated runoff across vegetation types are likely to be primarily a result of the influence of vegetation on evapotranspiration.

SUMMARY AND CONCLUSIONS

This study was intended to address the relative influence of space-time variability of rainfall and soil moisture—a variable that is influenced by land cover—on runoff generation in the Mekong river basin. To resolve this question we applied the VIC hydrologic model, and diagnosed various aspects of simulated runoff and streamflow over the Mekong basin. Our analysis shows that:

(1) While much of the runoff variability in the Mekong River basin results from the monsoonal precipitation regime and terrain topography, and in the dry season is dominated by snowmelt from China, a significant portion of this variability is explained by the simulated spatial patterns of soil moisture, which often do not follow precipitation patterns. Simulated soil moisture peaks lag behind precipitation peaks especially in the deepest soil layer, and soil moisture dynamics are controlled by evapotranspiration extraction from deep roots (mostly forest), infiltration from above, and base-flow. The upper layers show shorter lag relative to precipitation.

(2) The influence of simulated soil moisture on simulated runoff is exerted primarily through base-flow, but also through quick-flow. This was the case for Mekong sub-regions of contrasting geophysical and climatic characteristics, and is a result of that in VIC, base-flow is governed by lower zone storage, while quick-flow depends primarily on precipitation rate (though also on antecedent soil moisture in the relatively thin upper layer). The relative dependence was influenced by the slope and (calibrated) soil depth of a given sub-basin—factors that affect storage and drainage rates.

(3) Irrigation in the Mekong Delta, over parts of the Korat Plateau, areas surrounding the Tonle Sap Lake, and near the Mekong mainstream in Laos, has major effects on soil moisture. Bunded fields are used both in irrigated areas and in rainfed paddies. Because bunded fields retain surface runoff in ponded conditions, allowing re-infiltration and increased evapotranspiration, runoff generation is greatly reduced. This has important implications in the Korat Plateau where the use of earth bunds is widespread. The runoff in this region is notably low during the rain season. The region has an average annual runoff ratio of 0·15, which is considerably lower than the 0·43 average for Mekong River basin as a whole.

(4) Simulated soil moisture shows an important relationship to vegetation type: It was in general highest for agricultural areas; and lowest for grassland and woodland areas—except when antecedent precipitation was high (as is the case immediately following the rain season), when soil moisture was the lowest for forested areas. Thus, the vast forest to agriculture conversion that took place in the second half of the twentieth century was likely accompanied by an increase in soil moisture levels. Such an increase is exacerbated in those agricultural areas that are irrigated or where runoff is retained by bunds.

Rapid population growth and economic development over the past several decades in the Mekong River basin has placed increasing demands on the freshwater resources in this region. It is essential to determine how soil moisture, runoff and stream-flow may be impacted through land cover and land use change. This is the topic of a separate manuscript (Costa-Cabral *et al.*, to be submitted), where the calibrated VIC model used in the current manuscript is used to simulate the hydrologic response of hypothetical scenarios of land cover and use, and of future climate.

REFERENCES

Abdulla FA, Lettenmaier DP, Wood EF, Smith JA. 1996. Application of a macro-scale hydrologic model to estimate the water balance of the Arkansas-Red river basin. *Journal of Geophysical Research* **101**: 7449–4359.

Apichatvullop A. 1995. Hydrology of rainfed paddy land. Water Resources and Environment Institute. Faculty of Engineering. Khon Kaen University.

Barradas VL, Adém J. 1992. Albedo model for a tropical dry deciduous forest in western Mexico. *Biometeorology* **36**: 113–177.

Batjes NH. 1995. A homogenized soil data file for global environmental research: A subset of FAO, ISRIC and NRCS profiles (Version 1·0), Working Paper 95/10, ISRIC. ISRIC: Wageningen.

Blondin C. 1991. Parameterization of land-surface processes in numerical weather prediction. In *Land Surface Evaporation: Measurements and Parameterization*, Schmugge TJ, Andre JC (eds). Springer Verlag: New York; 31–54.

Bonan GB, Stillwell-Soller LM. 1998. Soil water and the persistence of floods and droughts in the Mississippi River Basin. *Water Resources Research* **34**: 2693–2701.

Brooks RH, Corey AT. 1966. Properties of porous media affecting fluid flow. *Journal of Irrigation and Drainage Division, American Society of Civil Engineering* **92**: 61–88.

Brutsaert W. 1975. Comments on surface roughness parameters and the height of dense vegetation. *Journal of the Meteorological Society of Japan* **53**: 96–97.

Carter AJ, Scholes RJ. 1999. *Generating a Global Database of Soil Properties*. Environmentek CSIR: Pretoria.

Cherkauer KA, Lettenmaier DP. 1999. Hydrologic effects of frozen soils in the upper Mississippi River basin. *Journal of Geophysical Research* **104**(D16): 19599–19610.

Christensen NS, Wood AW, Voisin N, Lettenmaier DP, Palmer RN. 2004. Effects of climate change on the hydrology and water resources of the Colorado River basin. *Climatic Change* **62**(1–3): 337–363.

Ducoudré NI, Laval K, Perrier A. 1993. SECHIBA, a new set of parameterizations of the hydrologic exchanges at the land-atmosphere interface with the LMD atmospheric general circulation model. *Journal of Climate* **6**: 248–273.

Delworth TL, Manabe S. 1988. The influence of potential evaporation on the variabilities of simulated soil wetness and climate. *Journal of Climate* **1**: 523–547.

Delworth TL, Manabe S. 1989. The influence of soil wetness on near-surface atmospheric variability. *Journal of Climate* **2**: 1447–1462.

Dümenil L, Todini E. 1992. A rainfall-runoff scheme for use in the Hamburg climate model. In *Advances in Theoretical Hydrology, A Tribute to James Dooge*, O'Kane JP (ed). European Geophysical Society Series on Hydrological Sciences, 1. New York: Elsevier; 129–157.

Entin JK, Robock A, Vinnikov KY, Hollinger SE, Liu S, Namkhai A. 2000. Temporal and spatial scales of observed soil moisture variations in the extratropics. *Journal of Geophysical Research* **105**(D9): 11865–11877.

European Commission. 2003. *South East Asia Regional Land Cover 2000 data set of the Global Land Cover 2000 database (GLC2000)*, European Commission, Joint Research Centre, Available at http://www-gvm.jrc.it/glc2000 (accessed June 2005).

Food and Agricultural Organization (FAO) of the United Nations. 1995. *Forest Resource Assessment 1990: Global Synthesis*. FAO Forestry Paper 124. FAO: Rome.

Fukui H, Chumphon N, Hoshikawa K. 2000. Evolution of rain-fed rice cultivation in northeast Thailand: increased production with decreased stability. *Global Environmental Research* **3**(2): 145–154.

Giambelluca TW, Fox J, Yarnasarn S, Onibutr P, Nullet MA. 1999. Dry-season radiation balance of land covers replacing forest in northern Thailand. *Agricultural and Forest Meteorology* **95**: 53–65.

Gray DM, Prowse TD. 1993. Snow and floating ice. In *Handbook of Hydrology*, Maidment DR (ed). McGraw-Hill: Columbus, OH; 7.1–7.58.

Haddeland I, Lettenmaier DP, Skaugen T. 2006. Effects of irrigation on the water and energy balances of the Colorado and Mekong River basins. *Journal of Hydrology* **324**: 210–223.

Hasselmann K. 1976. Stochastic climate models. Part I. *Theory. Tellus* **28**: 473–485.

Intergovernmental Panel on Climate Change (IPCC). 2001. *Climate Change 2001: Impacts, Adaptation and Vulnerability, Contribution of Working Group II to the Third Assessment Report of the IPCC*, McCarthy JJ, *et al.* (eds). Cambridge University Press: Cambridge; 944.

Jayawardena W, Mahanama SPP. 2002. Meso-scale hydrological modeling: application to Mekong and Chao Pharaya basins. *Journal of Hydrologic Engineering* **7**(1): 12–26.

Kalnay E, *et al.* 1996. The NCEP/NCAR 40-year reanalysis project. *Bulletin American Meteorological Society* **77**: 437–471.

Kite G. 2001. Modelling the Mekong: hydrological simulation for environmental impact studies. *Journal of Hydrology* **253**(1): 1–13.

Koster RD, Suarez MJ. 1995. Relative contributions of land and ocean processes to precipitation variability. *Journal of Geophysical Research* **100**: 13775–13790.

Liang X, Lettenmaier DP, Wood EF, Burges SJ. 1994. A simple hydrologically based model of land surface, water, and energy fluxes for general circulation models. *Journal of Geophysical Research* **99**(D7): 14415–14428.

Lohmann D, Nolte-Holube R, Raschk E. 1996. A large-scale horizontal routing model to be coupled to land surface parameterization schemes. *Tellus* **48A**: 708–721.

Lohmann D, Raschke E, Nijssen B, Lettenmaier DP. 1998. Regional scale hydrology: I. Formulation of the VIC-2L model coupled to a routing model. *Hydrological Sciences Journal* **43**: 131–141.

Matheussen B, Kirschbaum RL, Goodman IA, O'Donnell GM, Lettenmaier DP. 2000. Effects of land cover change on streamflow in the interior Columbia basin. *Hydrological Processes* **14**(5): 867–885.

Maurer EP, Lettenmaier DP. 2003. Predictability of seasonal runoff in the Mississippi River basin. *Journal of Geophysical Research* **108**(16): 8607.

Maurer EP, Wood AW, Adam JC, Lettenmaier DP, Nijssen B. 2002. A long-term hydrologically-based data set of land surface fluxes and states for the conterminous United States. *Journal of Climate* **22**: 3237–3251.

Mekong River Commission (MRC). 1997. *Mekong River Basin Diagnostic Study Final Report*. MRC: Bangkok.

Mekong River Commission (MRC). 2001. *Metadata for MRC Secretariat GIS Core Datasets*. MRC: Phnom Pehn.

Mekong River Commission (MRC) and World Wildlife Fund (WWF). 2003. *People and the Environment Atlas of the Lower Mekong Basin*. MRC Secretariat: Phnom Penh.

Nash JE, Sutcliffe JV. 1970. River flow forecasting through conceptual models part I—A discussion of principles. *Journal of Hydrology* **10**(3): 282–290.

Nijssen B, Schnur R, Lettenmaier DP. 2001a. Global retrospective estimation of soil moisture using the Variable Infiltration Capacity land surface model, 1980–93. *Journal of Climate* **14**(8): 1790–1808.

Nijssen B, Lettenmaier DP, Liang X, Wetzel SW, Wood EF. 1997. Streamflow simulation for continental-scale river basins. *Water Resources Research* **33**: 711–724.

Nijssen B, O'Donnell GM, Lettenmaier DP, Lohmann D, Wood EF. 2001b. Predicting the discharge of global rivers. *Journal of Climate* **14**: 3307–3323.

O'Donnell GM, Nijssen B, Lettenmaier DP. 1999. A simple algorithm for generating streamflow networks for grid-based, macroscale hydrological models. *Hydrological Processes* **13**: 1269–1275.

Payne JT, Wood AW, Hamlet AF, Palmer RN, Lettenmaier DP. 2004. Mitigating the effects of climate change on the water resources of the Columbia River basin. *Climatic Change* **62**(1–3): 233–256.

Pinker RT, Thompson OE, Eck TF. 1980. The albedo of a tropical evergreen forest. *Quarterly Journal of the Royal Meteorological Society* **106**: 551–558.

Rawls WJ, Ahuja LR, Brakensiek DL, Shirmohammadi A. 1993. Infiltration and soil water movement. In *Handbook of Hydrology*, Maidment DR (ed.). McGraw-Hill: Columbus, OH; 5.1–5.1.

Schaake J. 2000. Table published. Available at http://www.hydro.washington.edu/Lettenmaier/Models/VIC/Documentation/Info/soiltext.html (accessed June 2005).

Sellers PJ, Mintz Y, Sud YC, Dalcher A. 1986. A simple biosphere model (SiB) for use within general circulation models. *Journal of Atmospheric Sciences* **43**(6): 505–531.

Shepard DS. 1984. Computer mapping: The SYMAP interpolation algorithm. In *Spatial Statistics and Models*, Gaile GL, Willmott CJ (eds). D. Reidel Publishing Co.: Dordrecht; 133–145.

Shuttleworth WJ. 1993. Evaporation. In *Handbook of Hydrology*, Maidment DR (ed.). McGraw-Hill: Columbus, OH; 4.1–4.53.

Stibig H-J. 1997. (revised 1999). *Interpretation and Delineation from Satellite Images*, Technical Notes 2 of the Forest Cover Monitoring Project, a Co-operation project between the Mekong River Commission (MRC) and the Gesellschaft für Technische Zusammenarbeit (GTZ), Vientiane, Laos.

Su F, Xie Z. 2003. A model for assessing effects of climate change on runoff of China. *Progress in Natural Science* **13**(9): 701–707.

Su F, Adam JC, Trenberth KE, Lettenmaier DP. 2006. Evaluation of surface water fluxes of the pan-Arctic land region with a land surface model and ERA-40 reanalysis. *Journal of Geophysical Research* **111**(D5): D05110.

Van Rheenen NT, Wood AW, Palmer RN, Lettenmaier DP. 2004. Potential implications of PCM climate change scenarios for Sacramento, San Joaquin River basin hydrology and water resources. *Climatic Change* **62**(1–3): 257–281.

Vinnikov KY, Robock A, Speranskaya NA, Schlosser CA. 1996. Scales of temporal and spatial variability of midlatitude soil moisture. *Journal of Geophysical Research* **101**: 7163–7164.

Wu W, Geller MA, Dickinson RE. 2002. The response of soil moisture to long-term variability of precipitation. *Journal of Hydrometeorology* **3**: 604–613.

Yang D, Musiake K. 2003. A continental scale hydrological model using the distributed approach and its application to Asia. *Hydrological Processes* **17**(14): 2855–2869.

Zhu CM, Lettenmaier DP, Cavazos T. 2005. Role of antecedent land surface conditions on North American monsoon rainfall variability. *Journal of Climate* **18**(16): 3104–3121.